ELSEVIER

Chemical Engineering Journal 140 (2008) 562–569

Chemical Engineering Journal

www.elsevier.com/locate/cej

Numerical investigation on the flow characteristics and permeability of three-dimensional reticulated foam materials

Weigang Xu, Hongtao Zhang, Zhenming Yang, Jinsong Zhang *

Institute of Metal Research, Chinese Academy of Sciences, 72 Wenhua Road, Shenyang 110016, China

Received 23 August 2007; received in revised form 27 November 2007; accepted 6 December 2007

Abstract

In this paper, a three-dimensional (3D) model was proposed for predicting the flow characteristics and permeability of three-dimensional reticulated foam materials, which were prepared by replication process. Parameters, such as permeability, inertia coefficient, and friction factor, were obtained in order to describe the fluid flow characteristics of porous media. The influence of foam structure on the fluid flow characteristics was elucidated. Three flow regimes in porous media, including Darcy's regime, Forchheimer's regime and Froude's regime, were visualized and discussed. The flow transition from linear (Darcy's regime) to nonlinear (Forchheimer's regime) behavior, which is typical of experiments, was founded in the simulation. The data presented revealed the fact that the numerical results are in agreement with the experimental ones published previously.

Keywords: Finite volume analysis; Flow characteristics; Permeability; Inertial parameter; Friction factor; Foam materials

1. Introduction

The study of the creeping flow through porous media is fundamental in the prediction of seepage through filters and porous media. It is also important in the manufacturing of fiber-reinforced composites [1]. When the fluid flows past a porous matrix, it will run through the solid struts and a local turbulence can be produced by the eddies that are shed in the wake. Heat and mass transfer will be enhanced at the interfaces between the fluid and the struts. Thus porous media are widely applied in catalyst carriers [2], filters for molten metal [3] and component of compact heat exchangers [4–6].

Some parameters including permeability, inertial parameter and friction factor are often used to describe the physical properties for the fluid flow in porous media. Since the pioneering work of Darcy (1856) fluid flow in porous media has been extensively studied for the last 150 years. Until today, the Newtonian incompressible fluid flow at a steady state in the porous medium is commonly expressed by the parameters that are derived from two main equations: Darcy's law and Forchheimer's equation, shown in the following equations, respectively:

$$\frac{-\mathrm{d}P}{\mathrm{d}x} = \frac{\mu}{K}u \tag{1}$$

$$\frac{-\mathrm{d}p}{\mathrm{d}x} = \frac{\mu}{K}u + \frac{C_\mathrm{F}\rho}{\sqrt{K}}u^2 \tag{2}$$

where $-\mathrm{d}p/\mathrm{d}x$ is the pressure gradient along the flow direction, μ is the dynamic viscosity and ρ is the density of the fluid. The Darcian permeability K and inertial coefficient C_F are the characteristics of the porous media. Velocity u is called the superficial fluid velocity, defined by

$$u = \frac{Q}{A} \tag{3}$$

where Q is the volumetric flow rate and A is the exposed surface area of the porous media perpendicular to the flow direction.

When the energy loss is completely controlled by the viscous effects, the fluid at enough low Reynolds number can be expressed in Eq. (1) correctly. Under this condition the pressure gradient is found to be directly proportional to the flow velocity [7], which is usually called Darcian flow or seepage flow. As the velocities accelerated, the boundary layer becomes prominent and results in an "inertial core" [8]. The flow outside the boundary layers follows a nonlinear relationship between the pressure

* Corresponding author. Tel.: +86 24 23971896; fax: +86 24 23906640.
E-mail address: jshzhang@imr.ac.cn (J. Zhang).

1385-8947/$ – see front matter © 2007 Elsevier B.V. All rights reserved.
doi:10.1016/j.cej.2007.12.010

Nomenclature

A	area (m^2)
C_F	inertial coefficient
d	cell diameter (m)
d_p	pore diameter (m)
f	friction factor
K	permeability (m^2)
L	length (m)
P	pressure (Pa)
Q	volumetric flow rate ($m^3\ s^{-1}$)
Re_d	pore Reynolds number
Re_k	permeability Reynolds number
S	struts surface area of a single cell (m^2)
S_v	specific surface area (m^{-1})
u	velocity ($m\ s^{-1}$)
V	struts volume of a single cell (m^3)
V_0	total volume of a single cell (m^3)

Greek symbols

α	empirical parameter of Eq. (11)
β	empirical parameter of Eq. (11)
μ	dynamic viscosity ($kg\ m^{-1}\ s^{-1}$)
ε	porosity (%)
ρ	density ($kg\ m^{-3}$)

gradient and the flow rate, which is usually called non-Darcy flows. The non-Darcy flow is characterized by the prominent inertial effects that introduced the quadratic term, hence it also called inertial term in Darcy's law.

Flow characteristics are often defined by Reynolds number. In porous media, there are two methods for calculating the *Re* of a flow [9]. One is the permeability-based method (Eq. (4)). It is usually adopted when the permeability is relatively easily obtained, such as the researches of granular media; and it allows for the significance of $\sqrt{K}$ as the permeability-related length scale [10]:

$$Re_k = \frac{\rho u \sqrt{K}}{\mu} \tag{4}$$

The other considers that the pressure drop is controlled by specific surface area, which is the function of pore diameter. By substituting average pore diameter for the square root of the permeability it can be shown

$$Re_d = \frac{\rho u d_p}{\mu} \tag{5}$$

where d_p is the diameter of a circle with an area equivalent to the hexagonal window (Fig. 1b).

Fand et al. [8] and Kececioglu and Jiang [11] have pointed out the existence of three different flow regime based on the Reynolds number, defined in Eq. (5):

(i) Darcy's regime, or friction zone, where the flow is dominated by viscous forces.
(ii) Forchheimer's regime, or inertial zone, wherein the convective inertial terms of the local flow through the pores become significant.
(iii) Froude's regime, or turbulent zone, where the inertia terms are dominant and the movement is highly unsteady and chaotic.

A wide variety of experimental, analytical and numerical models, including two-dimensional (2D) and three-dimensional (3D), for porous media analysis has appeared in the literature. Andrade et al. [12] numerically simulated the flow character in a 2D model for disordered porous medium. The transition from linear to nonlinear flowing behavior was found at a scope of Reynolds number and such a transition can be understood and statistically characterized in terms of the spatial distribution of kinetic energy in the system. Boomsma et al. [9] adopted a 'wet' Weaire-Phelan foam model to study the pressure drop and flow characteristics in open cell metal foams. Based on the computational fluid dynamics method (CFD), Mills [13] computed the airflow permeability K for laminar flow in a wet Kelvin foam model and assumed K as the function of cell size and cell face hole size. At the same time, he concluded that the foam permeability is the function of the largest hole area in the cells. Lacroix et al. [14] used a cubic cell model studied the peculiar hydrodynamic behavior of SiC foams in chemical processes and validated their model by experimental results. Richardson et al.

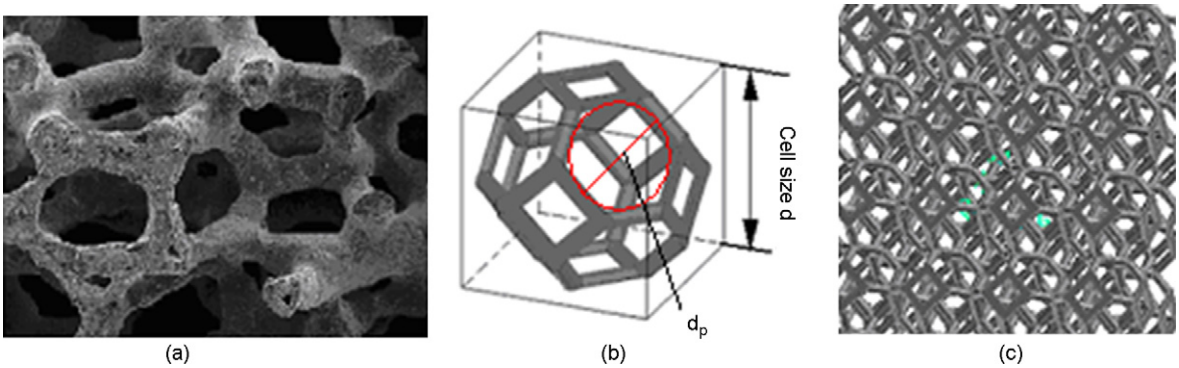

Fig. 1. (a) SEM images of SiC foam samples, (b) schematic view of tetrakaidecahedral cell for numerical simulations and (c) the bulk foam formed by tetrakaidecahedral cells packing.

[15], based on the work of Gibson and Ashby [16], consider that the cellular medium is formed by uniform tri-dimensional cell. Other investigating results can be seen in Refs. [17–19].

In the present study, the tetrakaidecahedron model was adopted and CFD method was used to systematically investigate the flow patterns in porous media and the relationship between fluid flow parameters and foams structure characteristics. A deviation from the classical Darcy law was also detected in the 3D model, just like the phenomina observed in Ref. [12]. The further study for heat and mass transport phenomena in porous media can be progressed by the numerical results provided in this paper.

2. Finite volume method analysis

2.1. Cell modeling

SiC foam ceramics were fabricated by polymer foam replication method [20] in Institute of Metal Research, Chinese Academy of Sciences. The scanning electron microscope (SEM) image of SiC foam was shown in Fig. 1a. For simulating the foam structure, the tetrakaidecahedron structure model was provided based on the formation of the foam in Fig. 1b. This structure is the only polyhedron that can stack the full space. Furthermore, it is in good agreement with the principle of the minimum surface energy. The tetrakaidecahedron structure is composed of six squares and eight hexagons. The struts of the real cells are represented by the cylinders with given diameters. The bulk foam structure was obtained using the arrays of the single cell in three spatial directions, exemplified in Fig. 1c. From Fig. 1a and b, it can be seen that the real structure of the cells have some similarities with the tetrakaidecahedron structure model. Hence, the cell shape represented in Fig. 1 can be considered as tetrakaidecahedron-shaped and the foam struts in the real and in the simulated are both cylinder-shaped. The difference between the two structures is that the real struts' surface is rougher than that of the simulated ones.

Based on the structure mentioned above, the porosity ε and specific surface area S_v of SiC foam is simply determined by

$$\varepsilon = \frac{V_0 - V}{V_0} \tag{6}$$

$$S_v = \frac{S}{V} \tag{7}$$

where V_0 is the total volume of a single cell and V and S are the volume and surface area that struts occupy.

2.2. CFD method

As for the flow of incompressible Newtonian fluid at steady state, the continuity and Navier–Stokes equations can be expressed as

$$\rho u \cdot \nabla u = -\nabla p + \mu \nabla^2 u \tag{9}$$

$$\nabla \cdot u = 0 \tag{10}$$

where μ and ρ are the viscosity and density of the fluid and u and p are local velocity and pressure, respectively.

CFD code **Fluent 6** was used to solve the equations mentioned above in porous media. The SIMPLE algorithm was used to couple the pressure and velocities. The second-order upwind advection model was used in the momentum dissipation equations. Fig. 2a exhibits a cell with its wall faces meshed by GAMBIT, a Fluent geometry and mesh generation software.

Using GAMBIT, the total volume of a single cell V_0, the struts volume V and struts surface S area can be calculated by integral. In Ref. [15], Richardson et al. proposed a correlation according the tetrakaidecahedra model produced by Gibson and Ashby. Similarly, according to the data obtained, we found the relationship between S_v, ε and d_p, based on present model is

$$S_v = \frac{6.702(1 - 1.003\sqrt{1-\varepsilon})}{d_p\sqrt{1-\varepsilon}} \tag{8}$$

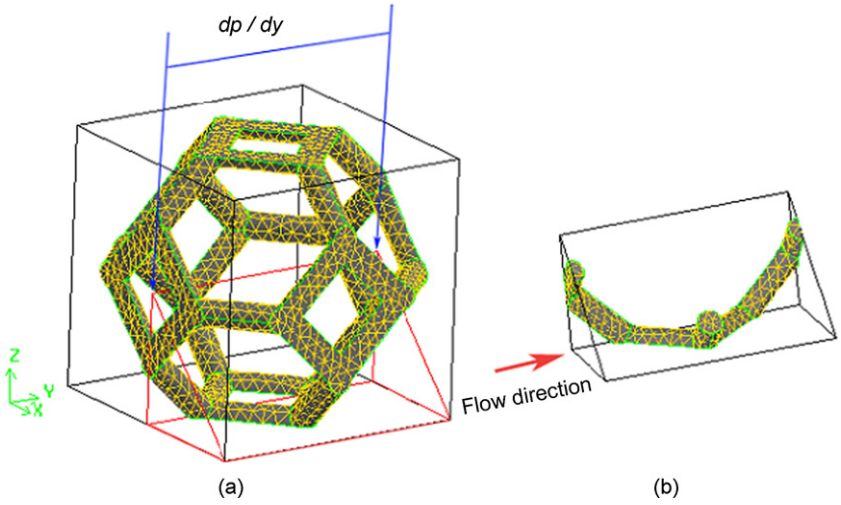

Fig. 2. Schematic view of periodic cells with wall meshed designed by computer in the numerical simulations. (a) 3D porous media and (b) 3D elementary fluid cell.

The geometric cell shown in Fig. 2a has so high symmetry that it is reasonable to choose a 1/8 element from the cell for numerical calculations, which simplifies the calculation, shown in Fig. 2b.

In order to simulate the infinite bulk of porous media, periodic boundary conditions were adopted at a pair of faces along with the y direction of the cell. The no-slip boundary condition was applied to the fluid/solid interface by default. At other faces, the slip-symmetry boundary conditions were carried out. Different pressure gradients were exerted on the y direction to obtain different velocities. For a given pressure, the fluid volumetric flow rate Q is determined by surface integral of periodic faces along flow direction. The superficial fluid velocity can be calculated in Eq. (3). The density and viscosity of the air, which was used as the fluid in the simulation, are 1.225 kg/m^3 and 1.7894×10^{-5} Pa s.

Various elements with unstructured mesh were calculated and showed grid independence of the results. The convergence criteria required a decrease of at least six orders of magnitude for the residuals with no observable change in the volume flow rate of the periodic boundaries.

3. Numerical results and discussion

3.1. Permeability and its influence factors

In order to obtain the permeability and inertial coefficient, Eq. (2) can be rewritten in the following form:

$$\frac{-\mathrm{d}p}{\mathrm{d}x} = \alpha u + \beta u^2 \tag{11}$$

where the unknown α and β are defined as follows:

$$\alpha = \frac{\mu}{K} \quad \text{and} \quad \beta = \frac{C_\mathrm{F}\rho}{\sqrt{K}} \tag{12}$$

For each model, the values of α and β are determined using a least squares fit. By plugging the values of α and β back into Eq. (12), the corresponding values for permeability K and inertia coefficient C_F can be obtained.

Permeability K of a porous material decides the difficulty for a fluid flowing through a porous medium by an applied pressure gradient. Hence, K can be treated as the fluid conductivity of the porous material. Permeability is strongly affected by two mean factors that are intrinsic characteristics of the porous medium. One is the porosity and the other is pore diameter. Fig. 3 illustrated that permeability generally increases with the porosity and pore diameter, but the increasing speed of permeability is not the same at different range of porosity. When a fixed cell size is selected, the permeability decrease more quickly at a relatively lower porosity than that at higher values. The reason is that the surface to volume ratio of a foam increases more rapidly at high porosity than that at low one (Fig. 4). The rapid increase of surface to volume ratio at high porosity results in a faster decrease of the pore diameter which leads to a stronger effect on the permeability. In conclusion, the permeability of the foams is more sensitive to their porosity when porosity values are much lower at a fixed cell size. From Fig. 5, it can also be seen that the permeability increase quickly with the cell size at a fixed porosity.

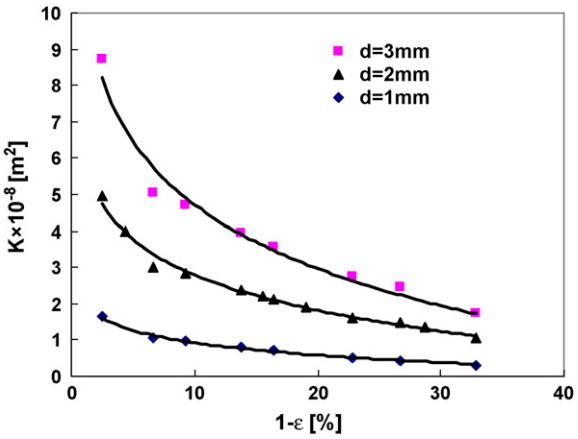

Fig. 3. Effect of porosity on the permeability in the foams at different cell diameters.

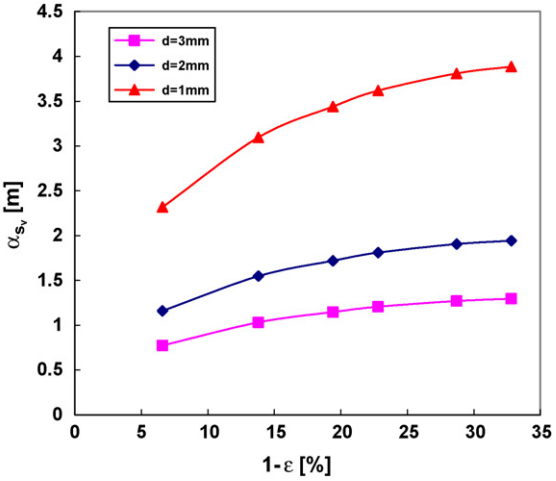

Fig. 4. Relationship between the porosity and specific surface area in the foams.

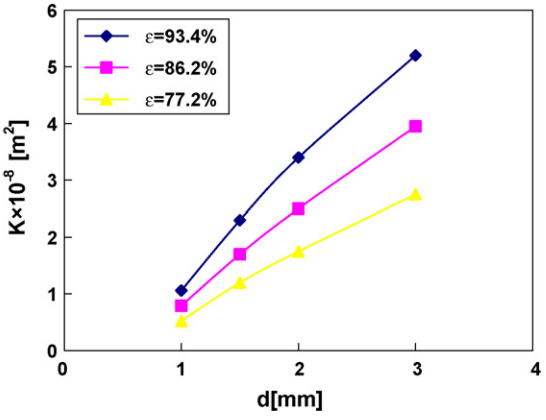

Fig. 5. Effect of cell diameter on the permeability in the foams at different porosities.

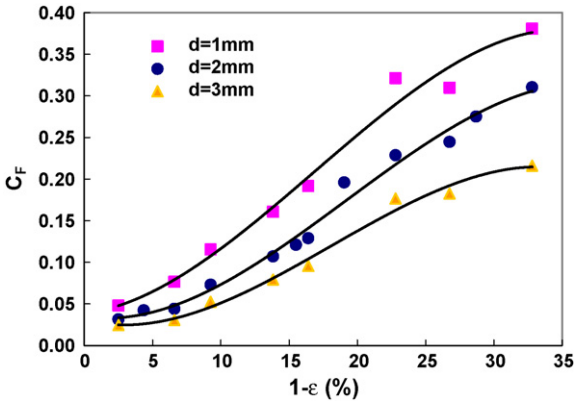

Fig. 6. Effect of porosity and cell diameter on inertial factor.

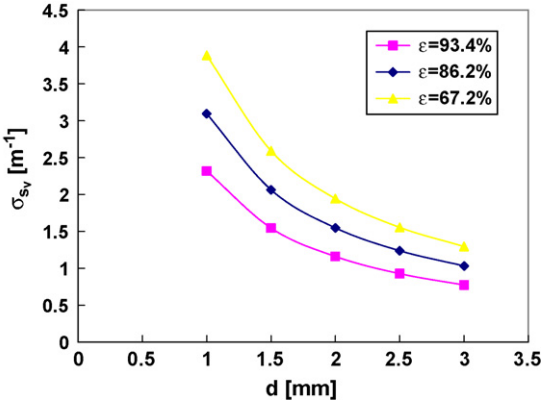

Fig. 8. Relationship between cell size and specific surface area in the foams.

3.2. Inertial coefficient C_F and its influence factors

The inertial coefficient C_F often uses to measure the drag experience during the fluid flow past the struts, so it is expected to strongly depend on the shape of the struts cross-section and the roughness of the surfaces. Contrary to the permeability, the inertial coefficients decrease with the increase of the porosity. The inertial value at small cell size is higher than that at large cell size when the porosity is fixed, exemplified in Fig. 6.

The inertial coefficients decrease more rapidly in the range of smaller cell size than that in the range of higher one, as shown in Fig. 7. This can be explained by the fact that the specific surface area of the foam decreases more rapidly in the range of small cell size, which was shown in Fig. 8. This means the quicker the increase of interfaces between the fluid and the strut is, the faster the enhancement of the drag force of the fluid is. In other words, the inertial effect of the foams is more sensitive to cell size when the cell size is relative small at a fixed porosity.

The best fit of α and β obtained was that utilizing the pore diameter, d_p, and the porosity ε as structural parameters. The final correlation, for SI units, has the following form:

$$\alpha = 5.64 \times 10^2 d_p^{0.709} (1-\varepsilon)^{-0.548} \frac{S_v^2 \mu (1-\varepsilon)^2}{\varepsilon^3} \quad (13)$$

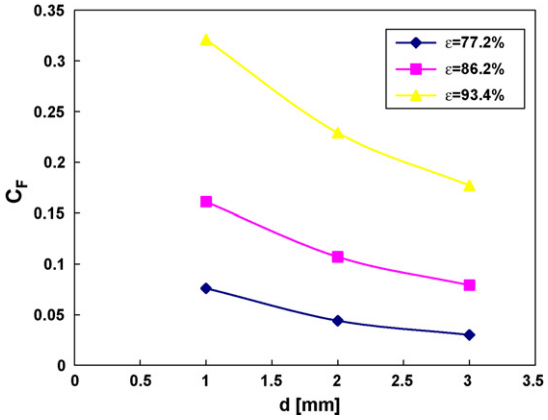

Fig. 7. Effect cell diameter on inertial factor.

$$\beta = 2.13 \times 10^2 d_p^{-0.783} (1-\varepsilon)^{0.426} \frac{S_v \rho (1-\varepsilon)}{\varepsilon^3} \quad (14)$$

3.3. Flow resistance and patterns

The results of the measured flow rate with applied pressure gradient were plotted in Fig. 9.

It can be found that the pressure drop increases as the flow rate increases. At fixed cell size, foam materials with the larger porosity tend to show small pressure drop, which is probably caused by the decrease of the inertia. The plot of $\varepsilon = 86.2\%$ in Fig. 9a is much steeper than that in Fig. 9b, which reveals the fact that the flow resistance decreases with the cell size at a fixed porosity. In general, these plots seemed to be quadratic in that the scale of the abscissa is not fine enough to embody the linear tendency at lower velocity zone.

In order to examine the flow transition at different Reynolds number, three cells with different values of porosity were chosen to calculate Re_k values in wide ranges. Rearranging Eq. (2) in the form,

$$f = \frac{1}{Re_k} + a \quad (15)$$

where $f \equiv (-dp/dx)\sqrt{K}/\rho u^2$ is the defined friction faction. The Reynolds number Re_k was defined in Eq. (4). And a is a constant to be determined and the inertial effect information is embedded in it [10]. In fact a is the C_F in Eq. (2). Thus we obtain a friction factor–Reynolds number type of correlation (Eq. (15)).

According to the data obtained in the above sections, by plugging the values of f, and Re_k into Eq. (15) the constant values of a can be obtained, three empirical correlations of f–Re_k relationship was developed.

$$f = \frac{1}{Re_k} + 0.056 \quad (16)$$

$$f = \frac{1}{Re_k} + 0.115 \quad (17)$$

$$f = \frac{1}{Re_k} + 0.224 \quad (18)$$

Fig. 10 shows the relationship between f and Re_k. It can be seen that f decreases as Re_k increases and the zone of the

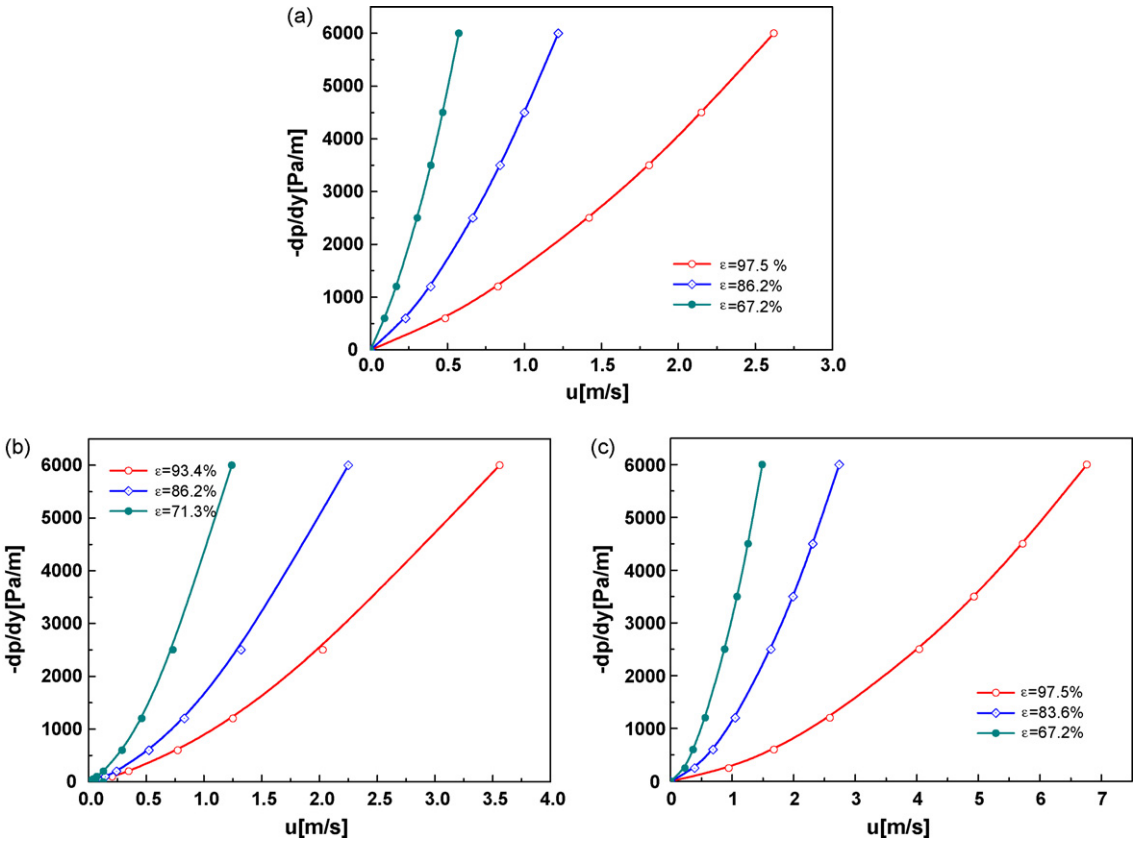

Fig. 9. Relationship between pressure gradient (dp/dy) and the superficial velocity u: (a) $d = 1$ mm, (b) $d = 2$ mm and (c) $d = 3$ mm.

transition between Darcy's and the strong inertial regimes is approximately $10^{-1} < Re_k < 6 \times 10^{-1}$, which reaches an agreement with the real flow experiments. But the transition value is different from Ref. [12], which is attributed to the different selected Reynolds numbers. Furthermore, it depends strongly on the nature of the porous media [10].

The different inertial effects, which corresponds to three different values of porosity, were reflected by different values of a. Three porosities are $\varepsilon = 93.4$, 86.2 and 67.2%, respectively. Thereafter, it also can be concluded from Fig. 10 that the inertial effect increases as the porosity decreases.

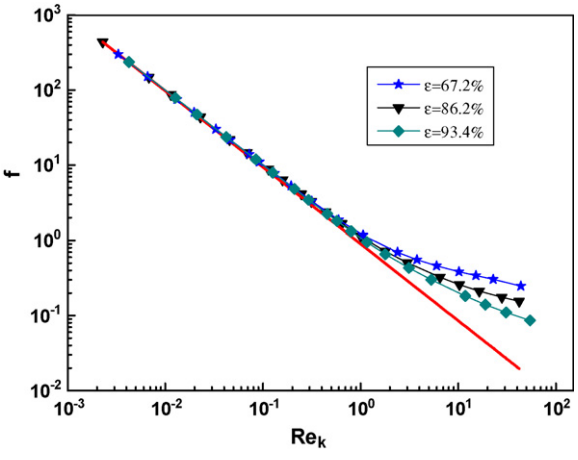

Fig. 10. Transition from linear flow to nonlinear flow and different inertial effect of different porosities.

Fig. 11 represented three different flow patterns mentioned above in porous media under different Reynolds numbers. Owing to the dominant viscous forces of the solid boundaries, the streamlines shown in Fig. 11a flows over the struts tightly and their geometry shapes are determined by the local geometry in porous media, which makes an agreement with Darcy's regime. When Re_d increases, the inertial forces become significant. This leads to the deviation of the streamlines that are not very circum-columnar and the formation of curves. The curves formed at high Re_d somewhat straighter than those at low Re_d. In Fig. 11b, this flow pattern falls into Forchheimer's regime. When $Re_d = 254$, the flow become unsteady and vortices are behind the struts, as shown in Fig. 11c. The vortices are unsteadily shredded to form the oscillations wakes behind the struts. This phenomenon is similar to the typical case that the fluid flows over a cylinder at a certain Re, because both of them have the shedding vortices by which the kormon's vortex streets can be formed behind the struts. However, the vortex streets in porous media will be disturbed with each other; meanwhile, the turbulence level in it is much more intense by the influence of the disordered struts and the complex geometry shapes of the porous media. Therefore, this is the reason why the heat and mass transfer is enhanced in porous media. This flow pattern apparently belongs to Froude's regime.

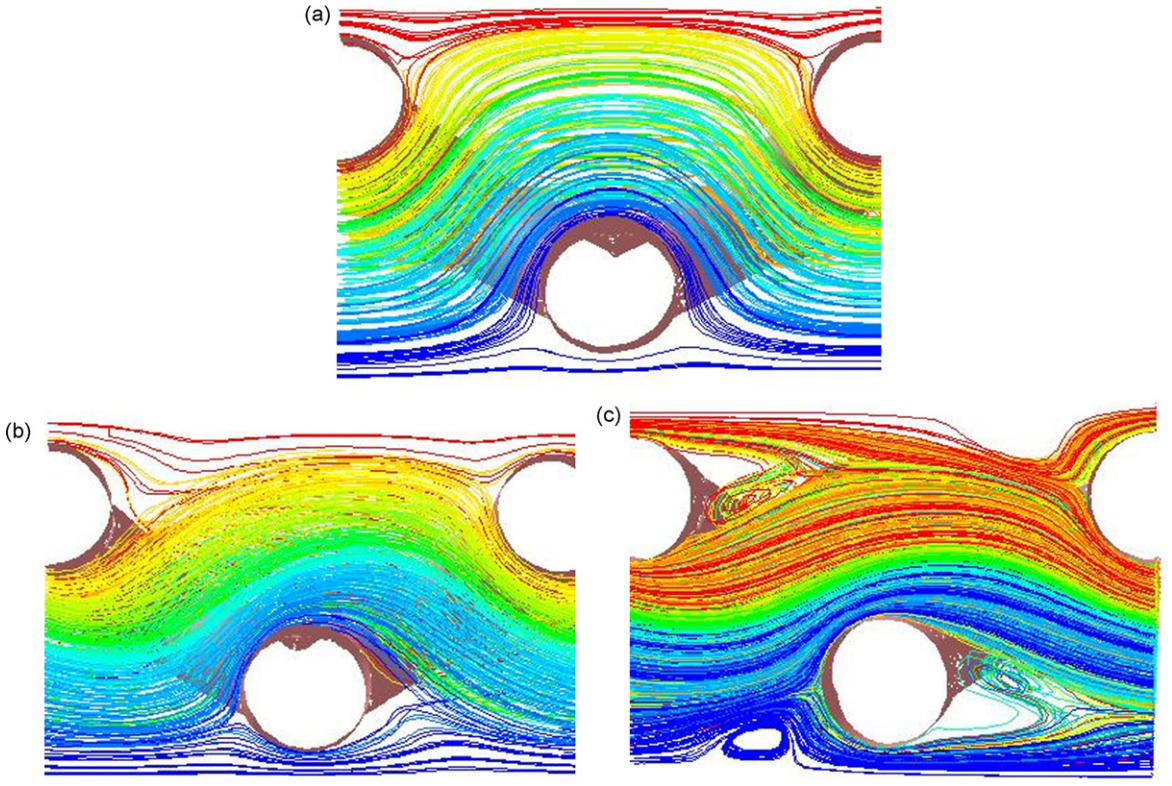

Fig. 11. Different flow patterns at different Re_d: (a) $Re_d = 0.55$, (b) $Re_d = 40$ and (c) $Re_d = 254$.

3.4. Comparison of experiments

Compared with experimental results, the plotted calculation results about (dp/dy)–u relationship of the foams was studied when the porosity of $\varepsilon = 90.75\%$ and $d = 1.8$ mm. The results were contrasted with other published results of Ref. [14].

From Fig. 12, it can be observed that the pressure value in our present paper and Ref. [14] are fitted well at low velocity scope (0–1.8 m/s). But with the increase of the velocity the calculated pressure value is generally lower at a fixed velocity than that of in Ref. [14], which the cell size of the foam are $d = 1.75$–1.8 mm and porosity $\varepsilon = 91\%$. As it mentioned above pressure drop is mainly dominated by viscous effect at low velocities. So the differences, such as average pore diameter, cross-section shape of struts, struts surface roughness, between our model and Ref. [14] not heavily influence the pressure drop across the test and calculated samples. Whereas with the increase of the velocity the factors which determined the inertial coefficient mentioned above become important which leads the noticeable inertial effect. So it can be assumed that the lower pressure gradient value in our study is due to the higher average cell diameter and the smoother surface of our model.

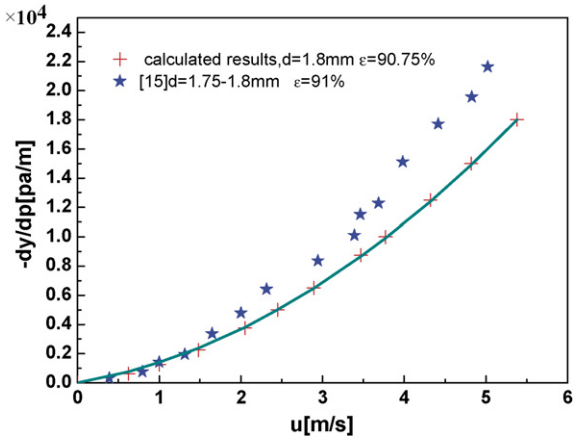

Fig. 12. Comparison between experiments and calculation results.

4. Conclusions

A tetrakaidecahedron structure model was introduced to simulate the characteristics of three flow regimes in 3D reticulated SiC foams. Parameters such as permeability, inertial coefficient and friction parameters were investigated in this paper. The Re_k range in which flow patterns transfer from linear to nonlinear in the porous medium was obtained. The variety of constant term values in f–Re_k correlations reflects the different inertial effects corresponding to different porosity at fixed cell size. The results showed that the permeability increases with the porosity and cell size. At fixed cell size, the permeability increases faster at low porosity range than it does at high porosity range. The permeability increases almost linearly with the cell size at fixed porosity. The inertial parameter decreases with the porosity and cell size, and at fixed porosity, it decreases more rapidly in the small cell size range than it does at large cell size range. Considering the differences between our model and the real one, the calculation results are in agreement with the published ones.

References

[1] C.Y. WangStokes, Slip flow through square and triangular arrays of circular cylinders, Fluid Dyn. Res. 32 (2003) 233–246.

[2] A.N. Pestryakov, A.A. Fyodorov, V.A. Shurov, M.S. Gaisinovich, I.V. Fyodorov, Foam metal catalysts with intermediate support for deep oxidation of hydrocarbons, React. Kinet. Catal. Lett. 53 (2) (1994) 347–352.

[3] F.A. Acosta, A.H. Castillejos, J.M. Almanza, A. Flores, An analysis of liquid flow through ceramic porous media used for molten metal filtration, Metall. Mater. Trans. B: Proc. 26 (1995) 159–171.

[4] L. Tadrist, M. Miscevic, O. Rahli, F. Topin, About the use of fibrous materials in compact heat exchangers, Exp. Therm. Fluid Sci. 28 (2004) 193–199.

[5] Q. Yu, A.G. Straatman, B.E. Thompson, Carbon-foam finned tubes in air–water heat exchangers, Appl. Therm. Eng. 26 (2006) 131–143.

[6] N. Delalic, D. Mulahasanovic, E.N. Ganic, Porous media compact heat exchanger unit—experiment and analysis, Exp. Therm. Fluid Sci. 28 (2004) 185–192.

[7] A. Bhattacharya, Thermophysical Properties and Convective Transport in Metal Foams and Finned Metal Foam Heatsinks, vol. 49, US Patent filed University of Colorado, 2001.

[8] R.M. Fand, B.Y.K. Kim, A.C.C. Lam, R.T. Phan, Resistance to the flow of fluid through simple and complex porous media whose matrices are composed of randomly packed sphere, ASME J. Fluids Eng. 109 (1987) 268–274.

[9] K. Boomsma, D. Poulikakos, Y. Ventikos, Simulations of flow through open cell metal foams using an idealized periodic cell structure, Int. J. Heat Fluid Flow 24 (2003) 825–834.

[10] J.W. Peak, B.H. Kang, S.Y. Kim, J.M. Hyun, Effective thermal conductivity and permeability of aluminum foam materials, Int. J. Thermophys. 21 (2) (2000) 453–464.

[11] I. Kececioglu, Y. Jiang, Flow through porous media of packed spheres saturated with water, Trans. AMSE J. Fluids Eng. 1116 (1994) 164–170.

[12] J.S. Andrade Jr., U.M.S. Costa, M.P. Almeida, H.A. Makse, H.E. Stanley, Inertial effects on fluid flow through disordered porous media, Phys. Rev. Lett. 82 (1999) 5249–5252.

[13] N.J. Mills, The wet Kelvin model for air flow through open-cell polyurethane foams, J. Mater. Sci. 40 (2005) 5845–5851.

[14] M. Lacroix, P. Nguyen, D. Schweich, C. Pham Huu, S. Savin-Poncet, D. Edouard, Pressure drop measurements and modelling on SiC foams, Chem. Eng. Sci. 62 (2007) 3259–3267.

[15] J.T. Richardson, Y. Peng, D. Remue, Properties of ceramic foam catalyst supports: pressure drop, Appl. Catal. A: Gen. 204 (2000) 19–32.

[16] L.J. Gibson, M.F. Ashby, Cellular Solids, Structures and Properties, Pergamon Press, Oxford, 1988.

[17] L. Giani, G. Groppi, et al., Mass-transfer characterization of metallic foams as supports for structured catalysts, Ind. Eng. Chem. Res. 44 (2005) 4993–5002.

[18] J.G. Fourie, J.P. Du Plessis, Pressure drop modelling in cellular metallic foams, Chem. Eng. Sci. 57 (2002) 2781–2789.

[19] F. Topin, J.P. Bonnet, B. Madani, L. Tadrist, Experimental analysis of multiphase flow in metallic foam: flow laws, heat transfer and convective boiling, Adv. Eng. Mater. 8 (2006) 890–899.

[20] R. Mouazer, I. Thijs, S. Mullens, et al., SiC-foams produced by gel casting: synthesis and characterization, Adv. Eng. Mater. 5 (2004) 340–343.